Laser interactions with embedded Ca metal nanoparticles in single crystal CaF_2

L. P. Cramer, B. E. Schubert, P. S. Petite, S. C. Langford, and J. T. Dickinson[a)]
Materials Science Program and Physics Department, Washington State University, Pullman, Washington 99164-2814

(Received 1 June 2004; accepted 10 January 2005; published online 23 March 2005)

Single crystal calcium fluoride (CaF_2) is an important material for vacuum-ultraviolet optics. Nevertheless, prolonged exposure to energetic radiation can color the material by producing calcium metal nanoparticles. We compare the effectiveness of laser conditioning treatments at wavelengths ranging from the near infrared to the deep ultraviolet in removing this coloration. Treatments at 157, 532, and 1064 nm can significantly reduce the visible coloration due to nanoparticles. In contrast, irradiation at 248 nm has little effect at fluences below the damage threshold for the material employed in this work. We present evidence that the effect of laser irradiation on coloration is principally thermal and is largely confined to the first 50 ns after each laser pulse. We attribute the wavelength dependence of the bleaching process to the wavelength dependence associated with Mie absorption by metal nanoparticles. The consequences of these observations with regard to laser conditioning processes in bulk optical materials are discussed. © *2005 American Institute of Physics*. [DOI: 10.1063/1.1862758]

I. INTRODUCTION

Defect production is a major impediment to the reliability of optical materials at high laser intensities—especially at ultraviolet (UV) wavelengths. These defects may be produced during prolonged service, as in the darkening of fused silica optical components at 248 and 193 nm.[1,2] In other cases, the relevant defects may be produced during crystal growth or manufacture, as in the case of large KH_2PO_4 crystals produced by rapid growth for the National Ignition Facility.[3,4] When damage is caused by absorption at defect aggregates, thermal or laser conditioning treatments can often improve the material quality prior to exposure to damaging laser intensities.[3,4] The mechanism driving this improvement is often not clear. An improved understanding of the relevant processes may facilitate the manufacture of more robust optical components and materials.[5]

Metal aggregates are readily produced in a number of materials by energetic radiation. In single-crystal CaF_2 (fluorite), calcium metal nanoparticles, often called colloids, are readily produced by relatively low energy electrons (2 keV) at modest doses (<5 mC/cm^2).[6] The resulting nanoparticles have diameters on the order of 20 nm, and form quasiorganized arrays near the surface.[7] These particles characteristically display an absorption peak near 600 nm that is well described in terms of Mie theory.[8–10] In many cases, the size and shape of the absorption peak can be analyzed to determine the approximate nanoparticle density and size distribution.[11] These nanoparticles serve as well-characterized aggregates for the study of laser conditioning treatments. We have recently shown that calcium nanoparticles are also generated by two photon absorption during exposure to modest fluences (~ 1 J/cm^2) of pulsed laser radiation at 157 nm.[12]

In this work, we compare the effect of pulsed laser radiation at 1064, 532, 248, and 157 nm on calcium nanoparticles produced in single crystal CaF_2 by electron irradiation. These wavelengths range from the near infrared to the vacuum UV regions of the spectrum. The greatest reduction in nanoparticle absorption was observed during exposure to 532 nm radiation, which is near the center of the nanoparticle absorption band. Significant reductions were also observed during exposure to 1064 and 157 nm radiation. In contrast, exposure at 248 nm had little effect on nanoparticle absorption at fluences below the damage threshold of the sample. We present evidence that the bleaching mechanism involves localized heating of the nanoparticles due to Mie absorption of the incident radiation.

II. EXPERIMENT

Vacuum UV grade single crystal CaF_2 was obtained from Korth Kristalle GmbH in the form of cylindrical rods, 1 cm in diameter. Two-millimeter thick slices were cleaved in air along the (111) plane. The samples were mounted on a vacuum-compatible, three-dimensional translation stage and positioned directly in front of an electron gun in vacuum ($\sim 1\times 10^{-7}$ Pa) for electron irradiation. The electron gun delivered 100 μA of 2 keV electrons on a 3×5 mm^2 area. After irradiation, the sample was removed from vacuum and mounted in a Perkin Elmer Lambda 900 spectrophotometer for absorption measurements.

In situ measurements of the change in absorption at 532 nm were made during bleaching treatments at 532 and 157 nm. Since 532 nm is near the peak of the nanoparticles absorption spectrum (see below), absorption at this wavelength provides an approximate indication of nanoparticle density.

[a)]Author to whom correspondence should be addressed; electronic mail: jtd@wsu.edu

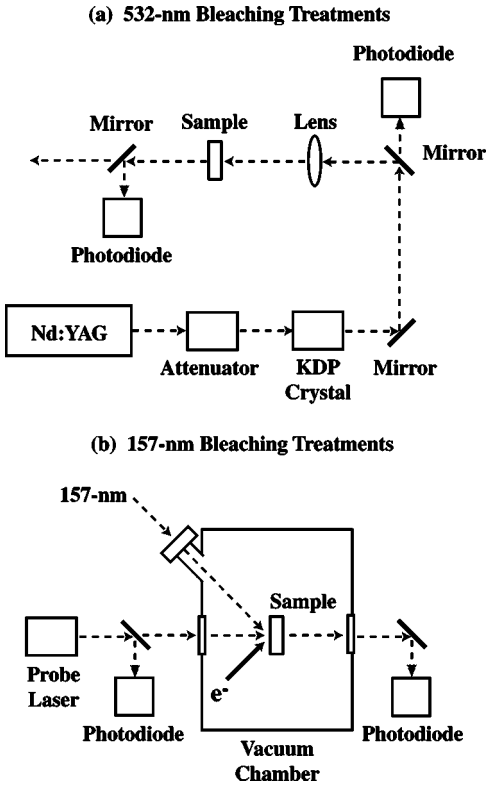

FIG. 1. Diagram of apparatus for real-time monitoring of nanoparticle bleaching during: (a) pulsed 532 nm irradiation in air and (b) pulsed 157 nm irradiation in vacuum.

The relevant experimental geometries are shown in Fig. 1. In each case, one photodiode probes the incident intensity, and a second probes the transmitted intensity. The photodiode outputs were digitized with a LeCroy LC334AL 500 MHz oscilloscope. The time response of the photodiodes and associated electronics was approximately 2 ns. The absorption was estimated from the ratio of the recorded photodiode signals.

Pulsed laser radiation at 1064 nm was provided by a Continuum Surelite II Nd: yttrium–aluminum–garnet (YAG) laser with a pulse width of 7 ns. This radiation was doubled to provide pulses at 532 nm. For *in situ* measurements of absorption change during 532 nm irradiation, pulse-to-pulse measurements of the incident and transmitted 532 nm intensities were used to monitor the evolution of nanoparticles absorption, as shown in Fig. 1(a). During bleaching treatments at other wavelengths, the beam of a doubled, cw Nd:YAG was directed through the sample and monitored as shown in Fig. 1(b). Pulsed laser radiation at 248 nm was provided by a Lambda Physik LEXtra 200 laser (KrF) with a pulse width of 30 ns. Radiation at 157 nm (F_2 excimer) was provided by a Lambda Physik LPF202 laser with a pulse width of 20 ns. Because 157 nm radiation is strongly absorbed by atmospheric oxygen and water, 157 nm exposures were performed in vacuum ($<1\times10^{-7}$ Pa). 157 nm pulses were transmitted from the laser to the vacuum system through a sealed tube purged with dry N_2.

III. RESULTS

Absorption spectra of CaF_2 exposed to 2 keV electrons at electron doses ranging from 6 to 72 mC/cm^2 at room temperature are shown in Fig. 2: Each sample shows a broad absorption band centered near 560 nm attributed to Mie absorption at calcium nanoparticles.[13,14] At the three higher doses, each spectrum also displays a shoulder just below 400 nm attributed to absorption at F centers (isolated fluorine vacancies with one trapped electron each). At electron doses above 50 mC/cm^2, the peak of the nanoparticle absorption shifts to longer wavelengths, consistent with Mie absorption by larger particles. These spectra are consistent with previous observations of nanoparticle absorption in radiation damaged and thermochemically reduced calcium fluoride.[13,14] The relatively weak F center absorption in irradiated calcium fluoride is consistent with the strong tendency of F centers to aggregate in this material. Near the peak of the nanoparticle absorption band, absorption by nanoparticles is much stronger than absorption due to point defects, even in samples exposed to electron doses as low as 6 mC/cm^2.

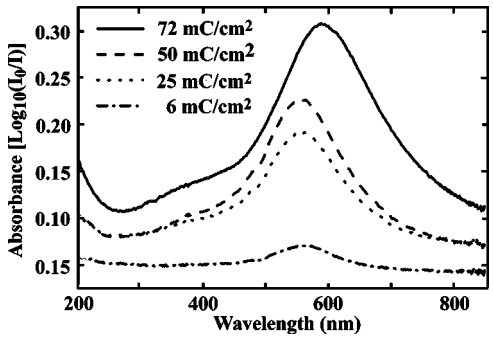

FIG. 2. Absorption spectra of cleaved CaF_2 as a function of electron dose. The increase absorption with increasing electron dose reflects increasing nanoparticle densities. The principal nanoparticle absorption peak shifts to longer wavelengths at the highest electron dose, reflecting an increase in the average nanoparticle diameter.

Subsequently exposing an electron-irradiated sample to pulsed 532 nm radiation can significantly reduce the absorption due to nanoparticles. Figure 3 shows absorption spectra of calcium fluoride samples treated with a high electron dose (greater than 100 mC/cm^2) before and after exposure to 50 mJ/cm^2 pulses of 532 nm radiation from Nd:YAG lasers. Significant changes in absorption are observed after ten laser pulses, with subsequent exposures producing further reductions. One thousand 532 nm laser pulses at this fluence reduced the absorption to approximately 5% of the initial value.

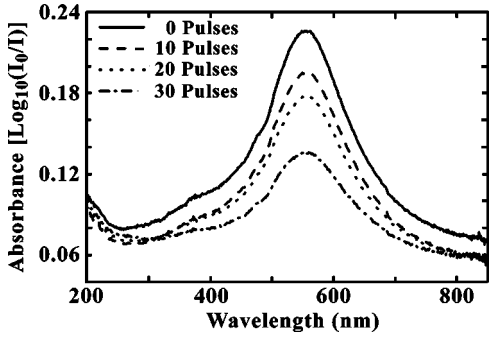

FIG. 3. Absorption spectra of electron-irradiated (100 mC/cm^2) CaF_2 subsequently exposed to 20 mJ/cm^2 pulses of 532 nm laser radiation. As the number of pulses of 532 nm radiation increases, the absorption drops.

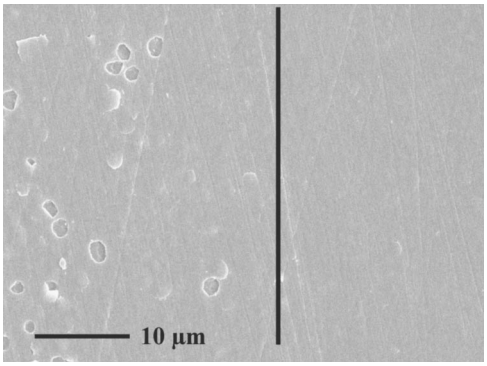

FIG. 4. SEM image of the edge of an electron-irradiated spot after a bleaching treatment at 532 nm. The left half of the image was exposed to both electrons and 532 nm radiation. The right half of the image was exposed to 532 nm radiation only.

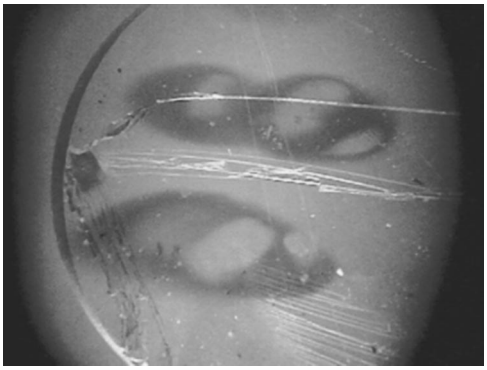

FIG. 6. Optical image of an electron-irradiated CaF_2 sample after several, localized bleaching treatments at 157 nm. The dark ovals were produced by electron irradiation. The clear spots in the ovals were produced by various 157 nm treatments.

Nanoparticle absorption can be reduced faster and more completely at higher laser fluences. For instance, 100 100 mJ/cm^2 pulses produced approximately the same reduction in nanoparticle absorption as 1000 50 mJ/cm^2 pulses. Unfortunately, treatments at fluences of 100 mJ/cm^2 and above significantly roughened the sample surface. A scanning electron microscope (SEM) image of an electron-irradiated surface subsequently exposed to 100 100 mJ/cm^2 pulses appears on the left hand side of Fig. 4. The entire imaged area was exposed to the 532 nm pulses, but only the left hand side of the image was exposed to electron irradiation. We attribute the pits to surface rupture by strongly heated, subsurface nanoparticles. Surface pitting could not be entirely avoided even at laser fluences as low as 20 mJ/cm^2.

In situ measurements of transmission near the center of the nanoparticle peak during exposure to 2 keV electrons and subsequent 157 nm pulses (20 Hz, 10 mJ/cm^2) appear in Fig. 5. Electron exposure continued for 10 min to a final dose of 400 mC/cm^2, and decreased the probe transmission from an initial value of 93% (due to reflection losses) to a minimum value of 57%. Subsequent laser irradiation restored the transmission of the probe beam to 74% over the course of some 50 000 pulses. The actual transmission in the 157 nm irradiated area was significantly higher. Because the area of the 532 nm probe beam on the sample ($\sim$0.1 cm^2) was significantly larger than the area of the focused 157 nm beam ($\sim$0.04 cm^2), the probe sampled a significant area outside the bleached region. Nevertheless, the kinetics of the bleaching process is clear. About 10 min (12 000 10 mJ/cm^2 pulses) are required to saturate the recovery. Absorption spectra of similar samples indicate that this laser treatment restores transmission to about 95% of the value before electron exposure.

A visual indication of the effectiveness of the bleaching process is given by the optical image in Fig. 6. The two dark, ovals were produced by electron-irradiation and appear purple in color photographs. The lighter regions within each oval were produced by various bleaching treatments—typically 1000 157 nm pulses at 100 mJ/cm^2. Relatively modest treatments can produce dramatic changes in transmission.

In general, bleaching was fastest at 532 nm, with slower bleaching at 1064 and 157 nm. However, even prolonged exposure to 248 nm radiation at the highest practical fluences (avoiding optical damage) had no significant effect on nanoparticle absorption. A summary of typical, 532 nm absorption before and after prolonged laser bleaching treatments at the four laser wavelengths is shown in Fig. 7.

Coloration due to point defects can often be reduced by photoelectronic transfer of charge from one defect to another (e.g., attaching or removing an electron). This mechanism is unlikely for extended metal nanoparticles. Indeed, prolonged

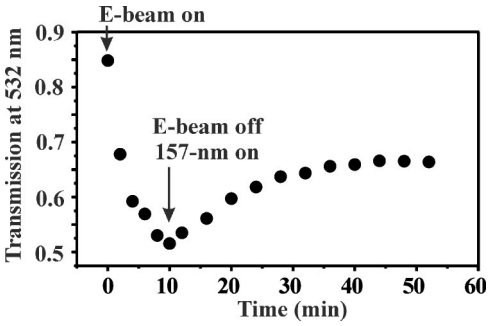

FIG. 5. Change of transmission at 532 nm during electron irradiation ($0 < t < 10$ min) and subsequent 157 nm irradiation. The area bleached by 157 nm radiation is significantly smaller than the 532 nm probe beam spot. Because the probe samples darkened material outside the laser spot, the transmission signal underestimates the increase in transmission during 157 nm exposure.

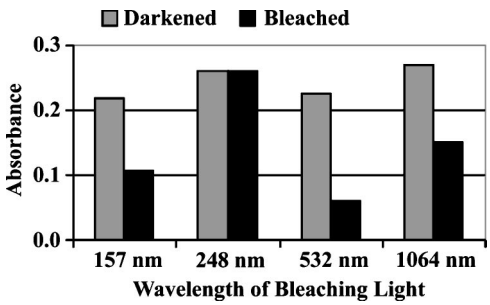

FIG. 7. Sample absorption at 532 nm after electron irradiation, before and after prolonged laser exposure at the four laser wavelengths. The laser exposures were: at 157 nm, 50 000 pulses at 150 mJ/cm^2; at 248 nm, 1000 pulses at 300 mJ/cm^2; at 532 nm, 1000 pulses at 50 mJ/cm^2; at 1064 nm, 1000 pulses at 200 mJ/cm^2.

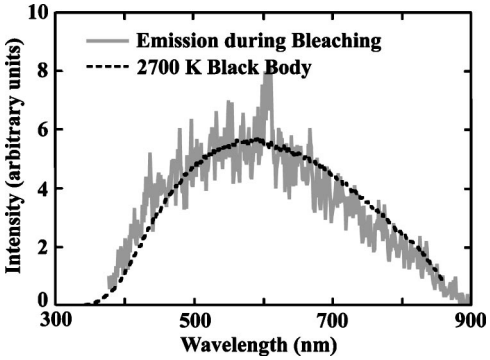

FIG. 8. Emission spectra acquired after the first laser pulse of a bleaching treatment at 1064 nm (light line). Spectral acquisition began a few nanoseconds after the laser pulse and continued for 1 μs. The broad continuum emission is consistent with blackbody radiation at a source temperature of 2700 K (dark, dotted line).

exposure to the cw 532 nm probe beam had no discernable effect on the absorption spectrum of electron-irradiated CaF_2; this same probe beam has strong effects on colored KCl, where charge transfer is an important bleaching mechanism. In contrast, metal nanoparticles in ionic crystals can often be removed by heat treatments.[10] Extreme heating should yield detectable visible and near-infrared blackbody radiation. To protect our detector, the longest available bleaching wavelength (1064 nm) was employed for blackbody measurements. Figure 8 shows an uncorrected spectrum of radiation accompanying the first pulse of 1064 nm laser light (30 mJ/cm^2) on a darkened crystal, where the detector was gated to start acquisition a few nanoseconds after the laser pulse and to end acquisition 1 μs later. The small peak near 600 nm in the laser induced spectrum is due to a calcium emission line, indicating the presence of a weak plasma at the sample surface. The corresponding blackbody temperature was estimated by acquiring a spectrum of a tungsten filament through the same optics and adjusting the filament current until a good match with the laser-induced spectrum was achieved. The filament temperature was then measured with an optical pyrometer. The dashed curve in Fig. 8 is the spectrum of the filament at a temperature of 2700 K. We conclude that the laser pulse has heated the nanoparticles to a temperature of about 2700 K.

The *in situ* absorption measurements can be acquired at high time resolution, allowing us to determine the timing of the absorption changes relative to the laser pulse. Figure 9 shows the transmission signal observed when electron-irradiated calcium fluoride is treated with single 1064 nm pulses at three different fluences. The insert shows the initial rise in transmission observed at a fluence of 550 mJ/cm^2. The rise time ($1/e$) of this increase is approximately 25 ns—significantly longer than both the laser pulse (7 ns) and time response of the detector/electronics (2 ns). As expected, larger transmission increases are observed at higher fluences. Similar measurements during exposure to 532 nm pulses at lower fluences (50–100 mJ/cm^2) yielded comparable changes in transmission.

Subsequent measurements of the absorption spectra of electron-irradiated samples treated with single 1064 nm pulses are shown in Fig. 10. Relatively high 1064 nm fluences were employed to produce a visible effect after one pulse. Spectra of samples before and immediately after electron irradiation are shown for comparison in curves (e) and (a), respectively. The laser-bleaching treatment not only decreases the nanoparticle absorption peak but also shifts it to shorter wavelengths—consistent with a modest decrease in the average nanoparticle size.

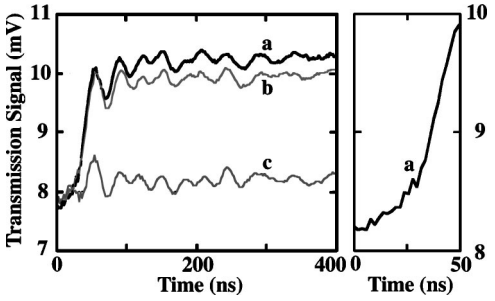

FIG. 9. Transmission change at 532 nm accompanying the first 1064 nm laser pulse on darkened material at three fluences: (a) 550 mJ/cm^2, (b) 400 mJ/cm^2, and (c) 275 mJ/cm^2. The inset shows the transmission change of (a) on an expanded time scale (550 mJ/cm^2 pulse).

IV. DISCUSSION

The electron-induced coloration observed in this work is consistent with the production and aggregation of F centers to form calcium metal nanoparticles.[11,13,14] Nanoparticle growth and shrinkage are facilitated by the close match between the volume per calcium atom/ion in calcium metal and calcium fluoride—with the calcium metal atoms requiring some 6% less volume. The resulting tensile stress on the nanoparticles is sufficient to modify their optical properties somewhat, but not enough to cause significant departures from a spherical shape. Little, if any, calcium diffusion is expected during nanoparticle formation. Rather, nanoparticles are formed by the diffusion of fluorine away from the particle; or equivalently, the aggregation of fluorine vacancies (F centers) at nanoparticle locations.

The formation of fluorine vacancies in calcium fluoride is accompanied by the formation of fluorine-rich defects, including H and I centers. (The H center is equivalent to an F_2^-

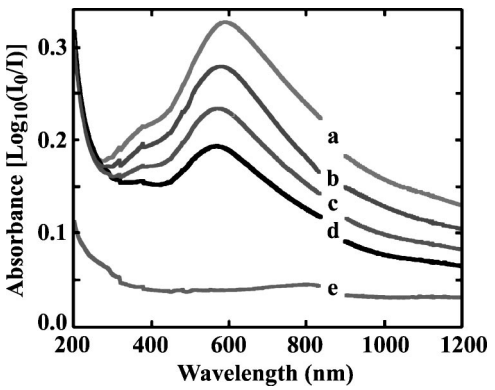

FIG. 10. Absorption spectra before and after the single-pulse, 1064 nm exposures of Fig. 9: (a) before 1064 nm exposure; (b) after one 275 mJ/cm^2 pulse; (c) after one 400 mJ/cm^2 pulse; (d) after one 550 mJ/cm^2 pulse; and (e) before electron and laser exposure. The gap in the data near 900 nm is due to a grating and light-source change during spectra acquisition.

ion occupying a fluorine lattice site, while the I center is an F_2^- ion at an interstitial site.) Some fluorine may occupy interstitial sites as neutral atoms or molecules.[15] In any case, little fluorine is lost from the lattice. Bleaching presumably involves the in-diffusion of interstitial fluorine (H centers) to nanoparticle positions, rather than the out-diffusion of fluorine vacancies. Electron transfer from metallic calcium to these interstitial fluorine defects ionizes Ca^0 to Ca^{2+} and restores the fluorite lattice.

Nanoparticle formation in CaF_2 has been studied by several groups.[7,14,16] Electron irradiation produces stable nanoparticles at room temperature.[17] Transmission electron microscopy (TEM) of irradiated material shows quasiorganized patterns of nanoparticles in the bulk.[7,18] Similar TEM observations of electron-irradiated CaF_2 in this laboratory show average particle diameters of about 20 nm in material exposed to 100 mC/cm^2 of 2 keV electrons.[19] This is consistent with the average particle diameters inferred from absorption spectra acquired by Huisinga *et al.* after similar electron exposures.[11]

Time resolved transmission measurements show that the majority of the bleaching occurs within a few tens of nanoseconds after the laser pulse (Fig. 9). Blackbody emission measurements indicate high temperatures ($\sim$2700 K in Fig. 8) are reached, at least at the high fluence end of the range employed in this work. These results are consistent with the shrinkage of nanoparticles by localized heating.

Pulsed laser radiation at 157, 532, and 1024 nm were effective in bleaching the nanoparticle absorption. Significantly, pulsed 248 nm radiation was ineffective, despite the fact that this wavelength lies between two wavelengths where significant bleaching was observed. This puzzling behavior is associated with an unusual optical property of the alkaline earth metals. Unlike most metals, calcium displays two bulk (and two surface) plasmons.[20,21] Plasmons play an important role in the absorption of metallic nanoparticles. The existence of two plasmons allows for the possibility of two strong absorptions, separated by a wavelength region with little absorption.

The wavelength dependence of absorption for small particles is readily calculated from the dielectric properties of the calcium/calcium fluoride system. As noted above, the average nanoparticle diameter in this work is approximately 20 nm. For particles much smaller than the laser wavelength, absorption dominates over scattering. This condition is well satisfied by particles with radius $a=10$ nm and wavelengths longer than 100 nm. Thus all the energy lost from the incident beam can be attributed to absorbed (as opposed to scattered) light.[22,23] The total energy ΔH absorbed by a nanoparticle of volume V and complex dielectric constant $\varepsilon=\varepsilon_r+i\varepsilon_i$, embedded in a transparent media of (real) dielectric constant ε_m, and exposed to radiation at wavelength λ and fluence (energy per unit area) F, is given by[22]

$$\Delta H = \left(\frac{6\pi VF}{\lambda}\right)\left(\frac{\varepsilon_i\varepsilon_m}{(\varepsilon_r+2\varepsilon_m)^2+\varepsilon_i^2}\right). \tag{1}$$

The dielectric properties of calcium metal have been fairly well studied. Unfortunately, these properties are significantly altered by the small size of the nanoparticles,[22] and the presence of significant tensile stresses.[9]

Orera and Alcacá have formulated an estimate of the effect of nanoparticle size and tensile stress on the dielectric constants of calcium metal in terms of the nearly free electron model. Although the electrons in calcium are strongly affected by factors neglected in this approximation, the model captures most of the physics responsible for the difference between calcium in nanoparticles and in the bulk.[10]

In the nearly free electron description, the dielectric constant of a bulk metal can be expressed as[10]

$$\varepsilon_r(E) = \varepsilon_0 - \frac{E_p^2}{E^2+E_0^2}, \tag{2}$$

$$\varepsilon_i(E) = \frac{E_p^2E_0}{E(E^2+E_0^2)}, \tag{3}$$

where E is the photon energy, ε_0 describes the contribution of ion core polarizability to the real part of the dielectric constant, and E_p is the plasmon energy. We note that the use of a free-electron plasmon energy is potentially ambiguous in an anomalous metal like calcium. Calcium has two bulk plasmons. Following Orera, we employ the energy of the low-energy plasmon. The constant E_0 describes the effect of the dielectric relaxation time.

The principal effect of confining electrons in the small volume of the nanoparticle is to decrease the relaxation time τ, the time between electron scattering events. In the nearly free electron model, the relaxation time is related to the bulk conductivity and the thermal electron mass. In pure calcium metal at room temperature, the mean relaxation time is $\tau_{\text{bulk}} \approx 4.2\times10^{-14}$ s. The corresponding energy ($E_0=\hbar\omega=\hbar/\tau$) is 0.016 eV—significantly smaller than the photon energies employed in this work. However, for sufficiently small particles, collisions with the surface will reduce the relaxation time. The mean time between scattering events at particle surfaces equals the electron (Fermi) velocity divided by the particle radius ($\tau_{\text{surface}}=a/\nu_F$). From Matthiessen's rule, the net scattering frequency is the sum of the bulk and the nanoparticle surface scattering frequencies. For nanoparticles,[10]

$$E_0^{\text{colloid}} = E_0^{\text{bulk}} + \frac{\hbar\nu_F}{a}. \tag{4}$$

Stress also alters the dielectric properties of the nanoparticles. The volume per calcium atom in the metal is about 6% less than the volume per calcium ion in calcium fluoride. Thus the calcium nanoparticles experience significant tensile stresses, on the order of 800 MPa. Orera and Alcacá estimate that this stress lowers the plasma frequency of the calcium particles by 10%. The change in ε_r and ε_i due to surface scattering and pressure effects can be estimated by subtracting the bulk values from Eqs. (2) and (3) with E_0 and E_p for calcium metal from the nanoparticle values formed by using the corrected values of E_0 and E_p in these same equations. In the limit of small (bulk) E_0, the resulting corrections become

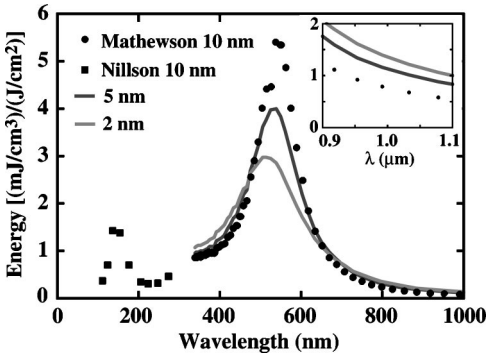

FIG. 11. Mie absorption per unit volume per unit fluence (dots) for metallic calcium particles of radius 10 nm embedded in a calcium fluoride matrix. The optical constants for metallic calcium were taken from Refs. 21 and 24. The lines show the predicted absorption for 5 mm (dark line) and 2 mm (light line) diameter particles. The predicted absorption near 1000 nm is displayed on an expanded vertical scale in the inset.

$$\Delta\varepsilon_r = \frac{0.188 * E_p^2}{E^2}, \tag{5}$$

$$\Delta\varepsilon_i = \frac{E_p^2}{E^3}\left[-0.188E_0 + 0.812\frac{\hbar\nu_F}{a} \right]. \tag{6}$$

These corrections were added to literature values for the dielectric constants for calcium metal, and the corrected values were employed in Eq. (1) to estimate the energy absorbed per particle as a function of energy and wavelength. Due to the difficulty of finding a reliable set of dielectric constants for calcium over the entire photon energy range employed, we have used values derived from reflection measurements by Nilsson and Forssell at photon energies greater than 3 eV,[21] and values derived from ellipsometric measurements by Mathewson and Meyers at lower photon energies.[24]

The energy absorbed per nanoparticle, per unit volume, per unit fluence, as a function of wavelength for particles of radius $a=10$ nm, is plotted as dots and squares in Fig. 11. The absorbed energy shows two peaks, corresponding to the two distinct plasmons in metallic calcium.[21] Both peaks are significantly shifted from the energies observed in bulk calcium due to nanoparticle size and pressure effects. The position of the low energy peak at 540 nm is consistent with the position of the nanoparticle peak in our absorption spectra (Fig. 2), and would account for strong nanoparticle heating at 532 nm. A second, smaller peak appears at 140 nm (beyond the range of our spectrophotometer). This would account for significant nanoparticle absorption at 157 nm, and contribute to increased UV absorption near 200 nm observed in darkened samples. The association between UV absorption and nanoparticle production in CaF_2 has not been previously made. The estimates of Fig. 11 suggest that a particle of radius 10 nm ($V=4.2\times10^{-24}$ m^3) exposed to a fluence of 100 J/m^2 would absorb about 6×10^{-15} J at 157 nm, 2×10^{-15} J at 248 nm, 23×10^{-15} J at 532 nm, and 0.25×10^{-15} J at 1064 nm.

Absorption estimates for the visible and near infrared regions are also shown in Fig. 11 for particles with radii of 5 nm (dark line) and 2 nm (light line). As the particle size decreases, the 540 nm peak broadens while maintaining (approximately) constant area. At wavelengths near 540 nm, the absorbed energy per unit volume is significantly lower for the smaller particles, but there is a range of wavelengths on both sides of the central peak where the smaller particles absorb more energy per unit volume than the larger particles. For instance, the estimated absorption per unit volume at 1064 nm increases 80% as the particle size decreases from 10 to 2 nm. As discussed below, this increase is a potential problem during laser conditioning operations.

The predicted Mie absorption is sufficient to produce significant heating. Assuming that the nanoparticles are spherical and heated uniformly throughout their volume, and that the thermal behavior can be approximated by room temperature values appropriate to CaF_2, the temperature change at the surface of the nanoparticle is given by[25]

$$\Delta T = \frac{\alpha A\Delta t}{kV}\left[2\,\mathrm{erfc}(0) + 2\,\mathrm{erfc}\left(\frac{a}{\sqrt{\alpha\Delta t}}\right) - \frac{4\sqrt{\alpha\Delta t}}{a} i^3\mathrm{erfc}(0) + \frac{4\sqrt{\alpha\Delta t}}{a} i^3\mathrm{erfc}\left(\frac{a}{\sqrt{\alpha\Delta t}}\right)\right], \tag{7}$$

where A is the power (energy per unit time—assumed to be constant during a laser pulse of duration Δt) delivered to a particle of radius $a=10$ nm and volume V. The quantity $(A\,\Delta t/V)$ corresponds to the product of the laser fluence and the absorbed energy per unit volume per unit fluence from Fig. 11. The erfc is the complementary error function, and the i^3erfc function is the result of three successive integrations of erfc. The i^3erfc function is defined and tabulated in Carslaw and Jaeger.[26] The room temperature thermal diffusivity and conductivity of CaF_2 are $\alpha=3.6\times10^{-6}$ m^2/s and $k=9.7$ W m^{-1} K^{-1}, respectively. On the time scale of the laser pulses used in this work, the scale length for heating $[d=(\alpha\,\Delta t)^{1/2}]$ ranges from 180 to 330 nm—1 order of magnitude larger than the particle radius. Thus the assumption that the contrasting thermal properties of the nanoparticle can be neglected is largely justified.

Applying these constants to a single embedded nanoparticle, the peak nanoparticle temperature change due to a single, 7 ns, 532 nm pulse at 50 J/m^2, is 3200 K. Similarly, the predicted temperature change for 100 J/m^2, 20 ns, excimer pulses is about 1600 K at 157 nm and 450 K at 248 nm. The temperatures at 532 and 157 nm are high enough to support thermal mechanisms for nanoparticle removal. However, the temperature change at 248 nm is low enough to preclude annealing effects. Orera *et al.* report a temperature of 430 K for the destruction of nanoparticles[10] produced by prolonged exposure to a 150 W Xe lamp; although this temperature is somewhat lower than the predicted temperature under 248 nm irradiation, significantly higher temperatures would be required to produce detectable changes in particle size during transient (tens of nanoseconds) laser-induced heating.

The estimates of Fig. 11 are not reliable at infrared wavelengths due to the limited range of available dielectric constant data.[21,24] The emission spectrum of Fig. 8 acquired at 1064 nm is the best evidence we can present that thermal annealing is possible at this wavelength. The spectrum corresponds to blackbody radiation at an effective temperature

of about 2700 K. Infrared absorption measurements in metallic calcium at this wavelength correspond to an absorption depth of about 15 nm.[27,28] Neglecting thermal conduction, exposing a 20 nm thick layer of calcium to 20 mJ/cm^2 of 1064 nm light would raise its temperature by roughly 3000 K, consistent with the data of Fig. 8. We therefore conclude that the observed nanoparticle bleaching due to laser treatments at the three wavelengths (157, 532, and 1064 nm) are thermal in nature, and that the loss of color is due to both removal and shrinkage of the initial nanoparticles.

In a typical laser conditioning scenario, the sample displays a range of defect sizes and thus a range of particle temperatures. If the particle temperature increases with particle size, as expected at 532 nm, the larger particles will be heated most effectively. As they shrink, the temperature change will drop and annealing will slow. To remove the smaller particles, the fluence must be raised. The fluence can be safely raised in this scenario as long as the size of the largest particles has been reduced to a safe value. Stepwise increases in fluence could in principle remove virtually all the nanoparticles while minimizing damage to the host material.

At 1064 nm, the majority (greater than 90%) of the bleaching was observed after the first laser pulse. This is likely a consequence of the particle size dependence on absorption. At wavelengths near 1000 nm, the inset in Fig. 11 suggests that small particles absorb more laser energy per unit volume than large particles. Therefore, any fluence sufficient to bleach the larger particles will produce a much larger temperature change in the smaller particles. In this case, a significant number of particles have been heated to temperatures near 2700 K. This degree of heating is likely to evaporate the smallest particles. The remaining, larger particles are not so strongly heated by subsequent pulses, and yield little, if any detectable blackbody radiation.

Material damage during laser conditioning should be much harder to avoid at wavelengths near 1064 nm, where absorption decreases with increasing particle size. As the largest particles shrink, they inevitably reach a size where they absorb strongly. Fluences sufficient to heat the large particles will overheat the small particles. This situation is inherently unstable and should be avoided to minimize damage of the host material. In some cases, the design wavelength for a set of optics may be unsuitable for laser conditioning and another, more suitable wavelength must be found. The choice of conditioning wavelength is often complicated by the lack of information on the relevant defects and how they are affected by the conditioning process.

In principle, simple laser conditioning can restore colored CaF_2 optics in some applications to a usable degree of transparency, as shown by the samples in Figs. 5 and 7. Due to the very high uniformity required for optical elements in photolithography, it is unlikely that such treatments would ever be sufficient for high resolution lithographic applications. However, CaF_2 in less demanding applications, including UV windows in high radiation environments (e.g., inertial fusion systems), may benefit from treatments to remediate radiation-induced defects. Doped CaF_2 is also a thermoluminescent material; the production of point defects by radiation and the effect of subsequent laser exposure is of considerable interest because it influences the performance of the material as a dosimeter or radiation counter when read with a laser.

V. CONCLUSION

Spectroscopic and single wavelength transmission techniques allow for the real-time monitoring of nanoparticle formation and destruction during electron and photon irradiation. To a large degree, these particles can be removed by carefully chosen laser exposures, although surface damage can be a problem. Blackbody emission measurements and Mie absorption calculations suggest that laser-induced nanoparticle heating is significant and are consistent with a photothermal bleaching mechanism. This heating drives recombination of metallic calcium with interstitial fluorine. Time resolved measurements of transmission at 532 nm indicate that the bleaching event occurs on time scales of tens of nanoseconds after the laser pulse. It is likely that similar, thermal processes break up defect aggregates in rapidly grown crystals of optical materials during laser-conditioning treatments prior to their first exposure to potentially damaging, high fluence radiation.[3,4] Although the optical properties of these aggregates are often poorly understood, they have important consequences as to the design of laser conditioning treatments such as *in situ* bleaching processes.

Our results to date do not show complete recovery of transmission. Significant improvements are expected if laser exposure at an appropriate wavelength begins at a low fluence which is then gradually raised. Further studies employing programmed cycles of laser fluence and wavelength, in conjunction with thermal treatments, could lead to successful restoration of colored CaF_2. Issues of changes in crystal structure around these radiation induced metal nanoparticles with laser treatment have been discussed in a recent publication.[19]

ACKNOWLEDGMENTS

This work was supported by the United States Department of Energy under Contracts DE-FG03-98ER14864 and DE-FG02-04ER15618. We thank Dr. Grant Norton and Joel LeBret, Washington State University, and Roland Bennewitz and Michael Reichling, Freie Universität Berlin, for helpful discussions.

[1] D. R. Sempolinski, T. P. Seward, C. Smith, N. Borrelli, and C. Rosplock, J. Non-Cryst. Solids **203**, 69 (1996).
[2] R. Schenker, F. Piao, and W. G. Oldham, in *Optical Micrography IX*, edited by G. E. Fuller (Society of Photo-Optical Instrumentation Engineers, Bellingham, Wa, 1996), Vol. 2726, pp. 698–706.
[3] M. J. Runkel, J. J. DeYoreo, W. D. Sell, and D. Milam, *Laser Conditioning Study of KDP on the Optical Sciences Laser Using Large Area Beams* (SPIE—The International Society for Optical Engineering, Boulder, CO, 1998), pp. 51–63.
[4] M. C. Staggs, M. Yan, and M. J. Runkel, in *Laser Raster Conditioning of KDP and DKDP Crystals Using XeCl and Nd:YAG Lasers* (SPIE—The International Society for Optical Engineering, Boulder, CO, 2001), pp. 400–407.
[5] H. Bercegol, *What is Laser Conditioning: A Review Focused on Dielectric Multilayers* (SPIE—The International Society for Optical Engineering, Boulder, CO, 1999), pp. 421–426.
[6] R. Bennewitz, C. Günther, M. Reichling, E. Matthias, S. Vijayalakshmi,

A. V. Barnes, and N. H. Tolk, Appl. Phys. Lett. **66**, 320 (1995).
[7]V. S. Teodorescu, L. C. Nistor, and J. V. Landuyt, in *Defects in Insulating Materials*, edited by G. E. Matthews and R. T. Williams (Trans Tech, Zurich, Switzerland, 1997), pp. 671–674.
[8]V. M. Orera and E. Alcalá, Phys. Status Solidi A **38**, 621 (1976).
[9]V. M. Orera and E. Alcalá, Phys. Scr. **44**, 717 (1977).
[10]V. M. Orera and E. Alcalá, Solid State Commun. **27**, 1109 (1978).
[11]M. Huisinga, N. Bouchaala, R. Bennewitz, E. A. Kotomin, M. Reichling, V. N. Kuzovkov, and W. v. Niessen, Nucl. Instrum. Methods Phys. Res. B **141**, 79 (1998).
[12]L. P. Cramer, S. C. Langford, and J. T. Dickinson (unpublished).
[13]F. Beuneu and P. Vajda, J. Appl. Phys. **78**, 6989 (1995).
[14]M. Reichling, Nucl. Instrum. Methods Phys. Res. B **101**, 108 (1995).
[15]R. Bennewitz, M. Reichling, and E. Matthias, Surf. Sci. **387**, 69 (1997).
[16]R. Bennewitz, D. Smith, M. Reichling, E. Matthias, N. Itoh, and R. M. Wilson, Nucl. Instrum. Methods Phys. Res. B **101**, 118 (1995).
[17]B. G. Ravi and S. Ramasamy, Int. J. Mod. Phys. B **6**, 2809 (1992).
[18]L. W. Hobbs, J. Phys. (Paris) **37**, 3 (1976).
[19]J. B. LeBret, L. P. Cramer, M. G. Norton, and J. T. Dickinson, J. Appl. Phys. **85**, 4382 (2004).
[20]C. Kunz, Z. Phys. **196**, 311 (1966).
[21]P. O. Nilsson and G. Forssell, Phys. Rev. B **16**, 3352 (1977).
[22]W. T. Doyle, Phys. Rev. **111**, 1067 (1958).
[23]M. Born and E. Wolf, *Principles of Optics*, 4th ed. (Pergamon, Oxford, 1970).
[24]A. G. Mathewson and H. P. Meyers, Phys. Scr. **4**, 291 (1971).
[25]J. C. Jaeger, Aust. J. Sci. Res., Ser. A **5**, 1 (1952).
[26]H. S. Carslaw and J. C. Jaeger, *Conduction of Heat in Solids*, 2nd ed. (Oxford, London, 1959).
[27]R. Blanc and R. Rivoira, C. R. Hebd. Seances Acad. Sci., Ser. A B, Sci. Math. Sci. Phys **265**, 1044 (1967).
[28]M. R. Potter and G. W. Green, J. Phys. F: Met. Phys. **5**, 1426 (1975).